ACS APPLIED MATERIALS & INTERFACES

Research Article

www.acsami.org

Dye-Sensitized Solar Cells Employing Doubly or Singly Open-Ended TiO_2 Nanotube Arrays: Structural Geometry and Charge Transport

Jongmin Choi, Seulki Song, Gyeongho Kang, and Taiho Park*

Department of Chemical Engineering, Pohang University of Science and Technology, San 31, Nam-gu, Pohang, Kyoungbuk 790-780, Korea

Supporting Information

ABSTRACT: We systematically investigated the charge transport properties of doubly or singly open-ended TiO_2 nanotube arrays (DNT and SNT, respectively) for their utility as electrodes in dye-sensitized solar cells (DSCs). The SNT or DNT arrays were transferred in a bottom-up (B-up) or top-up (T-up) configuration onto a fluorine-doped tin oxide (FTO) substrate onto which had been deposited a 2 μm thick TiO_2 nanoparticle (NP) interlayer. This process yielded four types of DSCs prepared with SNTs (B-up or T-up) or DNT (B-up or T-up). The photovoltaic performances of these DSCs were analyzed by measuring the dependence of the charge transport on the DSC geometry. High resolution scanning electron microscopy techniques were used to characterize the electrode cross sections, and electrochemical impedance spectroscopy was used to characterize the electrical connection at the interface between the NT array and the TiO_2 NP interlayer. We examined the effects of decorating the DNT or SNT arrays with small NPs (sNP@DNT and sNP@SNT, respectively) in an effort to increase the extent of dye loading. The DNT arrays decorated with small NPs performed better than the decorated SNT arrays, most likely because the $Ti(OH)_4$ precursor solution flowed freely into the array through the open ends of the NTs in the DNT case but not in the SNT case. The sNP@DNT-based DSC exhibited a better PCE (10%) compared to the sNP@SNT-based DSCs (6.8%) because the electrolyte solution flow was not restricted, direct electron transport though the NT arrays was possible, the electrical connection at the interface between the NT array and the TiO_2 NP interlayer was good, and the array provided efficient light harvesting.

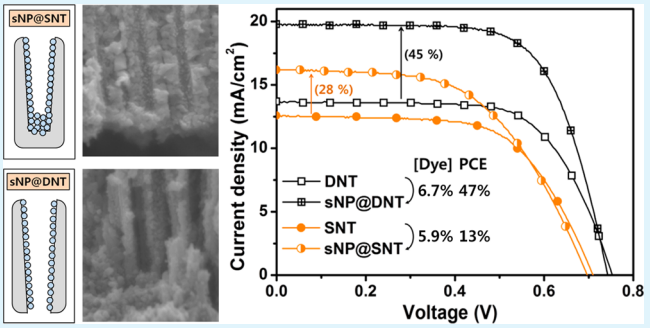

KEYWORDS: *TiO_2 nanotube arrays, doubly open-ended, singly open-ended, hybrid structure, structural geometry, charge transport*

INTRODUCTION

Nanocrystalline titanium dioxide (TiO_2) is frequently used as a photoanode material in dye-sensitized solar cells (DSCs) due to its excellent electrical properties and high thermal and chemical stability.[1−6] Mesoporous TiO_2 films composed of nanometer-sized particles provide a large surface area for anchoring high numbers of sensitizers.[7] However, random photoinduced electron diffusion through a disordered architecture increases the possibility of interfacial recombination with oxidized species (e.g., I_3^-) or cationic sensitizers.[8] Recombination is one of the main factors limiting the photovoltaic performance of a DSC.[9] Well-aligned one-dimensional (1-D) nanostructures, such as nanowires,[10] nanorods,[11] and nanotubes,[12] offer promising alternatives to the randomly distributed nanoparticle (NP) photoanodes.[13] A 1-D structure is advantageous in that it provides a direct pathway along which to collect the photoinduced electrons. TiO_2 nanotube (NT) arrays form vertically aligned structures with a large inner surface area. Zwilling et al. reported a pioneering electrochemical anodization approach that has since become the most widely used method for fabricating vertically oriented TiO_2 NT arrays.[14] Frank et al. demonstrated that charge recombination among photoinduced electrons was retarded in anodic NT arrays.[15] Therefore, highly ordered TiO_2 NT arrays are anticipated to provide an alternative electron transport material with a lower charge recombination rate and a higher electron collection efficiency relative to conventional disordered TiO_2 NP channels.[16]

Despite the outstanding properties of NTs, DSCs employing a Ti substrate bearing NTs that had been fixed through anodization exhibited very low power conversion efficiencies (PCE) of 1.9−6.89%[17−20] because the opaque Ti substrate required back-side illumination. New approaches, including the use of free-standing NT arrays with closed ends formed by detaching the NTs from the Ti substrate, have been tested in DSCs.[21,22] The DSCs prepared with such closed-ended (or singly open-ended NT (SNT)) arrays yielded PCEs as high as 8.07%.[23] The PCEs, however, were lower than those of the corresponding conventional DSCs prepared using TiO_2 nanoparticles (NP). Recently, Schmuki et al. reported the

Received: June 19, 2014
Accepted: August 19, 2014
Published: August 19, 2014

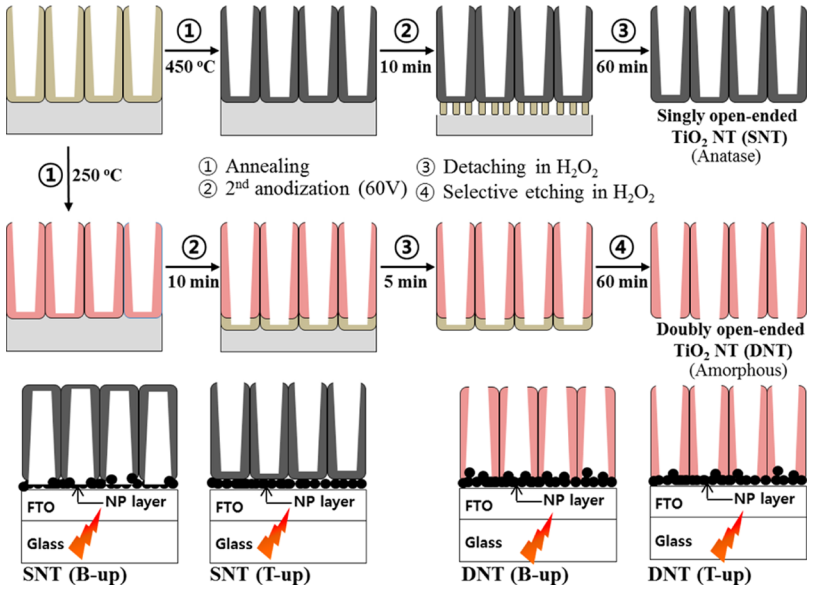

Figure 1. Schematic illustration of the preparation of the singly open-ended TiO_2 nanotube (SNT) and doubly open-ended TiO_2 nanotube (DNT) arrays, and the four types of DSCs prepared with SNTs (B-up or T-up) or DNTs (B-up or T-up).

preparation of doubly open-ended NT arrays.[24] Diau et al. applied the doubly open-ended TiO_2 NT (DNT) arrays to DSCs and achieved a PCE of 6.24%.[25] Huang et al. exhibit a PCE of 6.3% for a DSC using TiO_2 DNT, NP and NR (nanorod) hybrid electrode.[26] Chien et al. reported a PCE of 9.1% for a DSC employing DNT arrays that were 63 μm thick. These arrays provided a performance comparable to that obtained using conventional NP-based DSCs.[27]

DNT-based DSCs generally yield higher PCEs than SNT-based DSCs. The reasons underlying this performance difference have not been elucidated. The low PCE of SNT-based DSCs may result from the inefficient flow of electrolytes into the closed-ended SNT array layer. The closed ends could restrict the penetration of electrolytes into the inner region of the NT arrays. Electron transport may depend on the electrical connection between the NT arrays and the TiO_2 NP interlayer, which may be poor in the SNT arrays. The electrical connection is likely to be important for increasing the PCE. NPs appear to infiltrate the inner regions of open-ended DNT arrays, but not SNT arrays, to form strong connections between the DNT arrays and the NPs.

Here, we report the preparation of DSCs using DNT or SNT arrays. We systematically investigated the structural geometry and charge transport in these DSCs to determine why DNT-based DSCs display a higher PCE than SNT-based DSCs. DNT and SNT arrays decorated with small NPs (sNP@DNT and sNP@SNT, respectively) were prepared in an effort to enhance the light harvesting properties by increasing the dye loading capacity. The DNT arrays may have been more easily decorated with small NPs using a $Ti(OH)_4$ precursor solution[28−30] compared to the decoration of the SNT arrays because the precursor solution was able to flow freely into the arrays through the open ends. The small NPs covered the DNT array surfaces more easily than they did the SNT array surfaces. Therefore, in addition to improving the redox flow from the photoanode to a counter electrode and electrical connections at the interface between the NT arrays and the TiO_2 NPs interlayer, the sNP@DNT-based DSCs may provide direct electron transport though the NT arrays, enhanced light harvesting, and a higher PCE.

RESULTS AND DISCUSSION

TiO_2 NT arrays were grown through direct anodization of a Ti foil at room temperature in an ethylene glycol solution containing 0.3 wt % NH_4F under a 60 V DC potential over 120 min. Doubly open-ended TiO_2 NT arrays (Figure 1)[29] were prepared after the first anodization step by annealing the resulting membrane at 250 °C for 2 h to achieve a physically and chemically stable amorphous phase. A second anodization step was applied at room temperature under a 60 V DC potential for 5 min to allow the first thick NT layer to connect to the second thinner NT layer.[29] The double-layered NT membrane was easily detached from the Ti foil by immersing the NT membrane into a 33 wt % H_2O_2 solution for 5 min. The membrane remained physically stable during the detachment process and did not curl. The upper first layer was more chemically stable than the second thin layer. The first layer had previously been annealed at 250 °C. Thus, the second thin layer could be easily and selectively removed by prolonged etching for 60 min to yield a DNT array. The process and properties of the doubly open-ended TiO_2 NT arrays are described in detail in a previous report.[31] Figure 2a shows a cross-sectional high resolution scanning electron microscopy (HR-SEM) image of the 11 μm thick DNT membranes. The thin second bottom layer of the membranes had been selectively removed using the simple selective etching process. The diameter of the top surface was 110 nm, larger than that of the bottom surface (60 nm), as shown in Figure 2a,b.

SNT membranes were prepared by ultrasonically washing the membrane in ethanol after the first anodization step (Figure 1) to remove the electrolytes. The membrane was then annealed at 450 °C for 120 min, then anodized again at room temperature by applying a 60 V DC potential for 10 min. After rinsing with ethanol, the secondary anodized Ti foil was then immersed in a 33% H_2O_2 solution for 60 min to resolve the amorphous TiO_2 underlayer. The NT array from the first layer was separated from the substrate to form a closed-ended

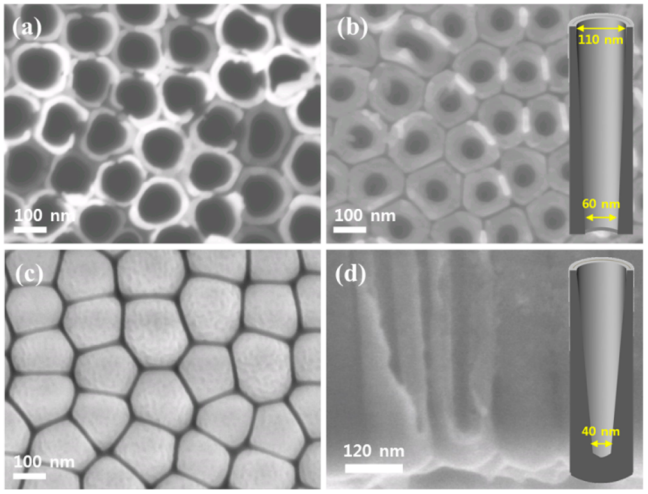

Figure 2. HR-SEM images: Top (a) and bottom (b) surfaces of the DNT arrays. Bottom (c) surface and cross-section (d) of the SNT arrays.

SNT array (Figures 2c,d). The inner diameter of the SNT ends was 30−40 nm, smaller than the inner diameter of the DNT ends.

The SNT and DNT membranes were transferred to a fluorine-doped tin oxide (FTO) substrate, onto which had been spread a 2 μm thick TiO_2 NP layer. Two methods of assembling the SNT or DNT arrays on the FTO glass substrate are available for preparing a front-illuminated DSC: the top surface upright method (denoted T-up) and the bottom surface upright method (denoted B-up) (Figure 1). The assembled electrodes were annealed at 550 °C for 30 min to induce the formation of good electrical connections between the NT arrays and the TiO_2 NPs. The TiO_2 NPs (and amorphous DNTs) were crystallized during this annealing step.[29] The electrodes were dye-sensitized by immersion in a 0.3 M ethanol solution of $(Bu_4N)_2Ru(dcbpyH)_2(NCS)_2$ (N719 dye) for 24 h. A semitransparent Pt-coated ITO counter electrode was used in the DSC. A liquid electrolyte solution,[32−34] composed of 0.03 M I_2, 0.6 M 1-butyl-3-methylimidazolium iodide (BMII), 0.1 M guanidinium thiocyanate, 0.5 M LiI, and 0.5 M 4-*tert*-butylpyridine in acetonitrile and valeronitrile (85:15) was introduced between the sensitized and counter electrodes using a syringe. The photovoltaic performances of the optimized devices were measured under AM 1.5 solar illumination (Figure 3) and are summarized in Table 1.

The highest PCE (6.8%), with a J_{SC} = 13.7 mA/cm^2, a V_{OC} = 0.752 V, and a FF = 0.663, was obtained in a DSC employing a B-up DNT array. These values were slightly higher than those obtained from a DSC employing a T-up DNT array, probably due to the difference between the inner diameters of the top (ca. 110 nm) and bottom (ca. 60 nm) surfaces. TiO_2 NPs 20 nm in size easily passed through the larger array openings. The interfacial gap between the DNT arrays and the TiO_2 NPs was filled to a greater degree in the B-up DNT arrays than in the T-up DNT arrays, as shown in Figure 4a,b. The interstitial filling formed good electrical connections between the DNT arrays and the TiO_2 NPs.

DSCs prepared from SNT arrays (denoted SNT-based DSCs) exhibited much lower photovoltaic activities than the DSCs prepared from DNT arrays (denoted DNT-based DSCs). Although the SNTs and the NPs formed good electrical connections, as observed in the DNT-based DSCs

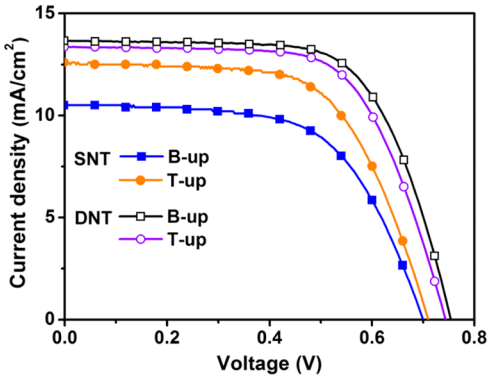

Figure 3. Photocurrent−voltage characteristics of the four types of DSCs employing SNT (B-up or T-up) or DNT (B-up or T-up) arrays under AM 1.5 irradiation.

Table 1. Photovoltaic Parameters for the Four types of DSCs Employing SNT (B-up or T-up) or DNT (B-up or T-up) Arrays under AM 1.5 Irradiation

TiO_2	t^a (μm)	Type^b	V_{OC} (V)	J_{SC} (mA/cm^2)	FF (%)	η (%)
DNT	11	B-up	0.752	13.7	0.663	6.8
DNT	11	T-up	0.740	13.4	0.656	6.5
SNT	11	B-up	0.699	10.5	0.608	4.5
SNT	11	T-up	0.711	12.6	0.620	5.5

^{a}Thickness of the NT arrays. The SNT or DNT arrays were placed on 2 μm thick TiO_2 NP layers (with NPs 20 nm in size). ^{b}T-up, top surface upright; B-up, bottom surface upright. Cell size: 0.25 cm^2 with black mask.

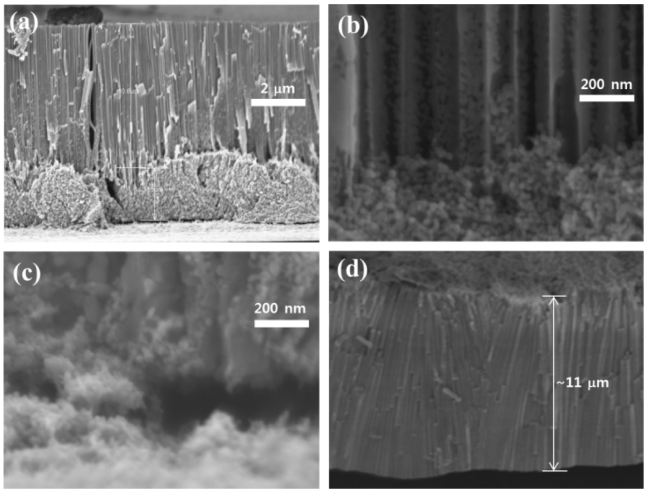

Figure 4. Cross-sectional HR-SEM images: (a) The DNT (B-up) arrays on the surfaces of the 2 μm thick TiO_2 NP layer. (b) The interface between the DNT (B-up) arrays and TiO_2 NPs. (c) The interface between the SNT (T-up) arrays and the TiO_2 NPs. (d) The SNT (T-up) arrays, showing that the bottom surface was not completely flat.

employing a B-up geometry, the SNT-based DSCs prepared with a B-up geometry exhibited the lowest photovoltaic activity, with a J_{SC} = 10.5 mA/cm^2, a V_{OC} = 0.699 V, and a FF = 0.608, giving a PCE of 4.5%. The poor performance was ascribed to the limitations in the redox efficiency resulting from the electrode geometry. I_3^- ions generated through dye regeneration by I^- inside the SNT arrays were required to migrate rapidly to the counter electrode or risk recombination with

photoinduced electrons on the SNT array surfaces. Recombination was apparent through a comparison of the FF values: 0.656 for B-up DNT versus 0.608 for B-up SNT. The resulting drop in J_{SC} (12.6 mA/cm^2 for B-up DNT versus 10.5 mA/cm^2 for B-up SNT) caused by the recombination reaction also decreased V_{OC}: 0.740 V for B-up DNT versus 0.699 V for B-up SNT, as reported by Frank et al.[35] V_{OC} is given by $(nkT/q) \times \ln(J_{SC}/J_S)$, where n is the device ideality factor, k is the Boltzmann constant, T is the temperature in Kelvin, q is the fundamental charge, and J_S is the saturation current density.[36] The low PCE in the SNT-based DSC prepared using a B-up geometry indicated that recombination reactions in the SNT array dominated the device performance.

The SNT-based DSCs employing a T-up geometry exhibited J_{SC} = 12.6 mA/cm^2, a V_{OC} = 0.7111 V, and a FF = 0.620, yielding a PCE of 5.5%, which is slightly larger than the value for the SNT-based DSCs prepared using a B-up geometry (4.5%), although this is smaller than the value for the DNT-based DSCs prepared using a B-up geometry (6.8%). Figure 4c shows a cross-sectional HR-SEM image collected at the interface between the SNT arrays and the 2 μm thick TiO_2 NPs. The image reveals the presence of a significant interfacial gap, which was generated after annealing at 550 °C for 30 min to crystallize the TiO_2 NPs. Unlike the other electrodes, the 20 nm sized TiO_2 NPs could not enter the SNT array prepared in the T-up geometry. Therefore, photoinduced electrons could not be effectively transferred from the ends of the SNTs to the TiO_2 NPs. Instead, the electrons accumulated at the ends of the SNTs. The bottom surface of the SNT arrays was slightly rougher than that of the DNT arrays as a result of the different detachment processes used for the two arrays (Figure 4d). The surface roughness resulted in a lower photovoltaic performance compared to the DNT-based DSCs prepared using a T-up geometry.

We further fabricated DSCs using DNT (B-up type) or SNT (T-up) arrays in an effort to improve the photocell efficiency. The electrodes were immersed in a 0.2 M acidic $Ti(OH)_4$(aq) prepared by adding $TiCl_4$ to water. The solution was then heated at 70 °C for 60 or 80 min, respectively, to induce the formation of TiO_2 NPs a few nanometers in size on the surfaces of the TiO_2 NTs. After the decoration step, the DNT (B-up type) or SNT (T-up) electrodes were reannealed to create small anatase TiO_2 NPs (denoted sNP@DNT or sNP@SNT, respectively).

Figure 5a,b shows top surface HR-SEM images of DNT (B-up) electrodes decorated with TiO_2 NPs a few nanometers in size, prepared by immersion in a 0.2 M acidic $Ti(OH)_4$(aq) for 60 or 80 min, respectively. The extent of decoration clearly increased with the immersion time. By contrast, the TiO_2 NPs aggregated on the edges of the SNTs arrays, as indicated by the arrows in Figure 5c. The aggregate sizes increased with the immersion time (Figure 5d), although small TiO_2 NPs did also grow on the side walls of the SNTs, as shown in the inset in Figure 5d. The TiO_2 NPs formed islands or very thin layers that possibly increased the dye loading.

Figure 6a shows the UV–vis absorption intensities of the N719 dye solutions after detaching the dyes from the TiO_2 electrodes in the presence of 0.1 M KOH. The dye-loading amount for each electrode was estimated by Beer–Lambert law, where the molar extinction coefficient of N719 is 1.4×10^4 M^{-1} cm^{-1} at 515 nm.[37] The dye-loading amount obtained from the DNT (0.104 μmol cm^{-2}) and SNT (0.101 μmol cm^{-2}) arrays were almost identical. After decorating the surfaces of the DNT

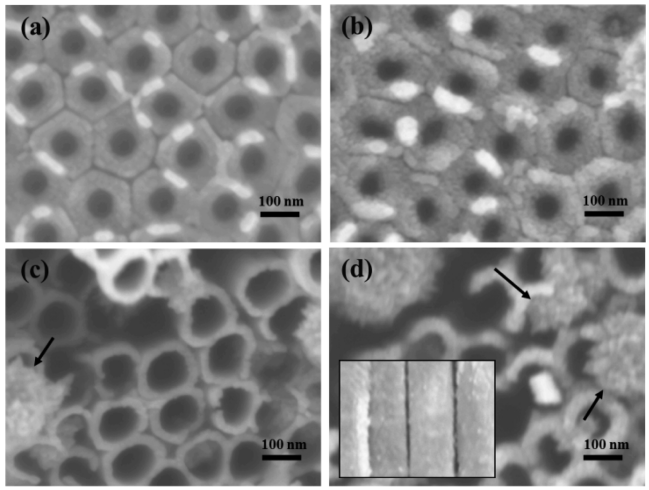

Figure 5. HR-SEM images: (a) Top surfaces of the sNP@DNTs (B-up, 60 min). (b) Top surfaces of the sNP@DNTs (B-up, 80 min). (c) Top surfaces of the sNP@SNTs (T-up, 60 min). (d) Top surfaces of the sNP@SNTs (T-up, 80 min). Inset: outside wall of the sNP@SNTs (T-up, 60 min).

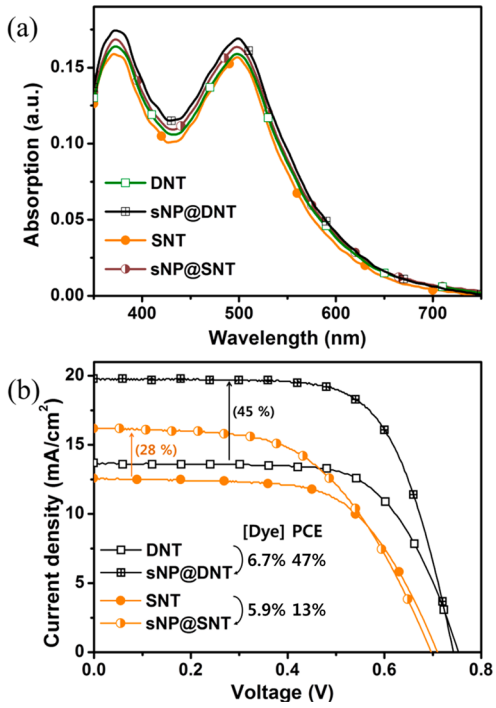

Figure 6. (a) UV–vis spectra of the N719 dyes detached from the electrodes using a 0.1 M KOH solution. (b) Photocurrent–voltage characteristics of four types of DSCs prepared using SNT, DNT, sNP@SNT, or sNP@DNT arrays under AM 1.5 irradiation.

or SNT arrays with the small TiO_2 NPs, the dye-loading amount (for the sNP@DNT and the sNP@SNT electrodes) increased slightly by 6.7% (0.111 μmol cm^{-2}) and 5.9% (0.107 μmol cm^{-2}), respectively. These results indicated that more dye molecules had adsorbed onto the larger surface areas of the electrodes due to decoration with the nanoparticles.

Figure 6b shows a comparison of the photocurrent–photovoltage (J–V) properties of the sNP@DNT and the sNP@SNT-based DSCs, along with their corresponding DNT and SNT-based DSCs (also see Table 2). The PCE values of the sNP@DNT and the sNP@SNT-based DSCs were 10.0 and

Table 2. Photocurrent−Voltage Characteristics of the DSCs Fabricated with Various TiO_2 NTs under AM 1.5 Irradiation

TiO_2	t^a (μm)	type[b]	V_{OC} (V)	J_{SC} (mA/cm^2)	FF (%)	η (%)
sNP@DNT[c]	11	B-up	0.744	19.8	0.676	10.0
sNP@SNT[c]	11	T-up	0.696	16.2	0.549	6.2

[a]Thicknesses of the NT arrays. The SNT and DNT arrays were placed on a 2 μm thick TiO_2 NP layer. [b]T-up, top surface upright; B-up, bottom surface upright. Cell size: 0.25 cm^2 with black mask.

6.2%, respectively, 47 and 13% greater than the PCE values of the corresponding DNT and SNT-based DSCs. The improvements mainly arose from the higher J_{SC} caused by the greater dye loading on the TiO_2 electrode surface. For example, the J_{SC} values of the DNT and SNT-based DSCs were 13.7 and 12.6 mA/cm^2, respectively. These values increased to 19.8 (45%) and 16.2 mA/cm^2 (28%), respectively. The remarkable increase of J_{SC} values in sNP@DNT and sNP@SNT electrodes might be affected by increased surface area but also enhanced the bonding between the TiO_2 and dye molecule,[38] and the connection between TiO_2 NP layers and TiO_2 NT films,[21] resulting in improved charge transfer.

The improvement in the PCE (13%) for the sNP@SNT was relatively small compared to the increase in J_{SC} (28%), as compared to the values obtained from the SNT array. These results arose mainly from the reduction in the FF (0.608, for the SNT, and 0.549, for the sNP@SNT). As mentioned previously (see Figure 2d), the inner diameter of the SNT narrowed in the bottom region. The sNPs in the SNTs were more aggregated in the narrow bottom region (Figure 7b) than

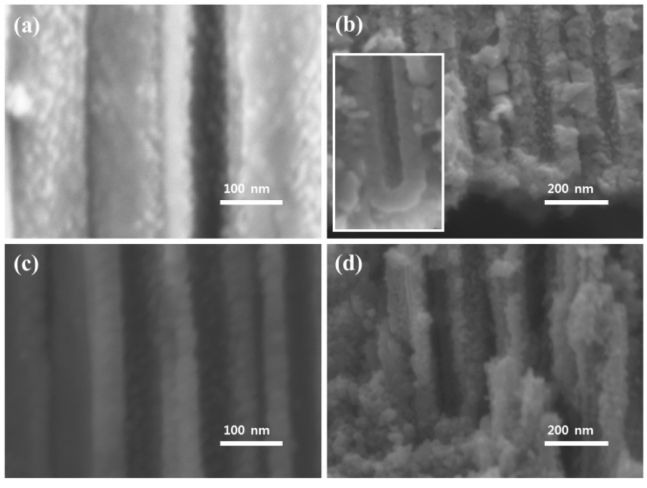

Figure 7. HR-SEM images: (a) Inside wall of the sNP@SNT. (b) Cross-sectional image of the bottom region of the sNP@SNT electrode. Inset: cross-sectional image of the bottom region of the SNT electrode. (c) Inside wall of the sNP@DNT. (d) Cross-sectional image of the bottom region of the sNP@DNT electrode. Immersion time in $Ti(OH)_4$: 60 min.

in the wide middle (or top) region (Figure 7a), unlike the sNPs in the sNP@DNT (Figure 7c,d). The inset in Figure 7b clearly shows the aggregated growth of sNPs in the SNTs. The aggregated sNPs in the narrow bottom region hampered the flow of electrolytes to the counter electrode, which enhanced recombination of the photoinduced electrons with I_3^-. We concluded that the decrease in FF resulted from clogging of the narrow bottom region by the aggregated sNP growth. This result was confirmed by fabricating sNP@SNT in $Ti(OH)_4$ for an extended immersion time. Indeed, the FF values decreased to 0.42 as the immersion time increased to 80 min (Figures S1 and S2, Supporting Information).

The photoinduced electron loss mechanism operating in the sNP@NT-based DSC was further investigated using electrochemical impedance spectroscopy (EIS).[39,40] Figure 8 shows

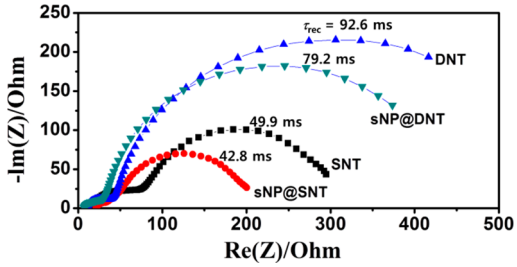

Figure 8. Nyquist plots for the SNT, DNT, sNP@SNT, and sNP@DNT-based DSCs, measured at −0.69 V in the dark. The recombination resistances (R2) were calculated by fitting to a simplified circuit (see the Supporting Information for details).

Nyquist plots of the DNT, sNP@DNT, SNT, and sNP@SNT-based DSCs, measured at −0.69 V in the dark. The recombination resistance (R_{rec}) between the DNTs and I_3^- was 515 Ω, much greater than the resistance between the SNTs and I_3^- (225 Ω). The electron recombination time (or lifetime, τ_{rec}) of the DNT-based DSC (τ_{rec} = 92.6 ms), which was calculated according to the equation $\tau_{rec} = 1/2\pi f_{max}$, where f_{max} is the frequency at the maximum theta, was longer than that of the SNT-based DSC (τ_{rec} = 49.9 ms). This result indicated that the photoinduced electron loss mechanism dominated the SNT-based DSC to a greater extent than it did in the DNT-based DSC due to incomplete contact between the TiO_2 NP interlayer and the SNT arrays. This result was consistent with the photovoltaic performances. Decorating the DNT or SNT arrays with the TiO_2 NPs slightly decreased R_{rec} (e.g., 515 Ω, DNT versus 405 Ω sNP@DNT; and 225 Ω, SNT versus 130 Ω, sNP@SNT) and the electron recombination time (τ_{rec} = 92.6 ms, DNT versus 79.2 ms sNP@DNT, and 49.9 ms SNT versus 42.8 ms sNP@SNT). The electron recombination times in the DSCs prepared using the NT arrays were significantly greater than those (27 ms) obtained using the conventional TiO_2 NPs (Figure S3, Supporting Information). Thus, the improved photovoltaic performance of the sNP@DNT-based DSC (or sNP@SNT), compared to the DNT-based DSCs (or SNT), mainly resulted from the higher dye loading.

CONCLUSIONS

In conclusion, (i) rapid electron transport at the interface between the TiO_2 NT array and the TiO_2 NP interlayer, and (ii) better electrolyte diffusion, thereby promoting the redox process, were found to be important for extracting electrons from a DSC and improving the FF value. A variety of DSC geometries were tested using SNT or DNT arrays. The presence of an even distribution of few nanometer-sized TiO_2 NPs decorating the inner and outer surfaces of the DNT arrays increased the dye loading (6.5% increase). The sNP@DNT-based DSC exhibited the best PCE (10%), representing an increase of 47% relative to the DNT-based DSC. The TiO_2 NPs formed aggregates on the edges and bottom areas of the SNT arrays. The aggregated NPs reduced the FF and charge

collection efficiency. The PCE of the sNP@SNT-based DSC was lower than that of the sNP@DNT-based DSC, although the PCE of the sNP@SNT-based DSC (6.2%) did improve relative to the SNT-based DSC (5.5%).

■ ASSOCIATED CONTENT

Supporting Information

Experimental section, characterization, $I-V$ characteristics of devices, the FF values as a function of the $TiCl_4$ treatment time, and Nyquist plots of electrochemical impedance spectrophotometer. This material is available free of charge via the Internet at http://pubs.acs.org.

■ AUTHOR INFORMATION

Corresponding Author

*T. Park. E-mail: taihopark@postech.ac.kr.

Notes

The authors declare no competing financial interest.

■ ACKNOWLEDGMENTS

This work was supported by the Nano-Material Technology Development Program (2012M3A7B4049989), the Center for Next Generation Dye-sensitized Solar Cells (No. 2008−0061903) and the Basic Science Research Program (No. 2012M1A2A2671699) through a NRF funded by MSIP (Korea).

■ REFERENCES

(1) O'Regan, B.; Grätzel, M. A Low-Cost, High-Efficiency Solar Cell Based on Dye-Sensitized Colloid TiO_2 Films. *Nature* **1991**, *353*, 737−740.

(2) Park, S.-H.; Lim, J.; Song, I. Y.; Atmakuri, N.; Song, S.; Kwon, Y. S.; Choi, J.; Park, T. Stable Dye-Sensitized Solar Cells by Encapsulation of N719-Sensitized TiO_2 Electrodes Using Surface-Induced Cross-Linking Polymerization. *Adv. Energy Mater.* **2012**, *2*, 219−224.

(3) Quintana, M.; Edvinsson, T.; Hagfeldt, A.; Boschloo, G. Comparison of Dye-Sensitized ZnO and TiO_2 Solar Cells: Studies of Charge Transport and Carrier Lifetime. *J. Phys. Chem. C* **2007**, *111*, 1035−1041.

(4) Park, S.-H.; Song, I. Y.; Lim, J.; Kwon, Y. S.; Choi, J.; Song, S.; Lee, J.-R.; Park, T. A Novel Quasi-Solid State Dye-Sensitized Solar Cell Fabricated Using a Multifunctional Network Polymer Membrane Electrolyte. *Energy Environ. Sci.* **2013**, *6*, 1559−1564.

(5) Lim, J.; Kwon, Y. S.; Park, T. Effect of Coadsorbent Properties on the Photovoltaic Performance of Dye-Sensitized Solar Cells. *Chem. Commun.* **2011**, *47*, 4147−4149.

(6) Lim, J.; Kwon, Y. S.; Park, S.-H.; Song, I. Y.; Choi, J.; Park, T. Thermodynamic Control over the Competitive Anchoring of N719 Dye on Nanocrystalline TiO_2 for Improving Photoinduced Electron Generation. *Langmuir* **2011**, *27*, 14647−14653.

(7) Nazeeruddin, M. K.; Kay, A.; Rodicio, I.; Humpbry-Baker, R.; Miiller, E.; Liska, P.; Vlachopoulos, N.; Grätzel, M. Conversion of Light to Electricity by cis-XzBis(2,2′-bipyridyl-4,4′-dicarboxylate)-ruthenium(II) Charge-Transfer Sensitizers (X= $C1^-$, Br^-, I^-, CN^-, and SCN^-) on Nanocrystalline TiO_2 Electrodes. *J. Am. Chem. Soc.* **1993**, *115*, 6382−6390.

(8) Law, M.; Greene, L. E.; Johnson, J. C.; Saykally, R.; Yang, P. D. Nanowire Dye-Sensitized Solar Cells. *Nat. Mater.* **2005**, *4*, 455−459.

(9) Fisher, A. C.; Peter, L. M.; Ponomarev, E. A.; Walker, A. B.; Wijayantha, K. G. U. Intensity Dependence of the Back Reaction and Transport of Electrons in Dye-Sensitized Nanocrystalline TiO_2 Solar Cells. *J. Phys. Chem. B* **2000**, *104*, 949−958.

(10) Feng, X.; Shankar, K.; Varghese, O. K.; Paulose, M.; Latempa, T. J.; Grimes, C. A. Vertically Aligned Single Crystal TiO_2 Nanowire Arrays Grown Directly on Transparent Conducting Oxide Coated Glass: Synthesis Details and Applications. *Nano Lett.* **2008**, *8*, 3781−3786.

(11) Jiu, J.; Isoda, S.; Wang, F.; Adachi, M. Dye-Sensitized Solar Cells Based on a Single-Crystalline TiO_2 Nanorod Film. *J. Phys. Chem. B* **2006**, *110*, 2087−2092.

(12) Grimes, C. A. Synthesis and Application of Highly-Ordered Arrays of TiO_2 Nanotubes. *J. Mater. Chem.* **2007**, *17*, 1451−1457.

(13) Zheng, Q.; Kang, H.; Yun, J.; Lee, J.; Park, J. H.; Baik, S. Hierarchical Construction of Self-Standing Anodized Titania Nanotube Arrays and Nanoparticles for Efficient and Cost-Effective Front-Illuminated Dye-Sensitized Solar Cells. *ACS Nano* **2011**, *5*, 5088−5093.

(14) Zwilling, V.; Aucouturier, M.; Darque-Ceretti, E. Anodic Oxidation of Titanium and TA6V Alloy in Chromic Media. An Electrochemical Approach. *Electrochim. Acta* **1999**, *45*, 921−929.

(15) Zhu, K.; Neale, N. R.; Miedaner, A.; Frank, A. J. Enhanced Charge-Collection Efficiencies and Light Scattering in Dye-Sensitized Solar Cells Using Oriented TiO_2 Nanotubes Arrays. *Nano Lett.* **2007**, *7*, 69−74.

(16) Liu, Z.; Misra, M. Dye-Sensitized Photovoltaic Wires Using Highly Ordered TiO_2 Nanotube Arrays. *ACS Nano* **2010**, *4*, 2196−2200.

(17) Zhu, K.; Vinzant, T. B.; Neale, N. R.; Frank, A. J. Removing Structural Disorder from Oriented TiO_2 Nanotube Arrays: Reducing the Dimensionality of Transport and Recombination in Dye-Sensitized Solar Cells. *Nano Lett.* **2007**, *7*, 3739−3746.

(18) Kuang, D.; Brillet, J.; Chen, P.; Takata, M.; Uchida, S.; Miura, H.; Sumioka, K.; Zakeeruddin, S. M.; Grätzel, M. Application of Highly Ordered TiO_2 Nanotube Arrays in Flexible Dye-Sensitized Solar Cells. *ACS Nano* **2008**, *2*, 1113−1116.

(19) Paulose, M.; Shankar, K.; Varghese, O. K.; Mor, G. K.; Hardin, B.; Grimes, C. A. Backside Illuminated Dye-Sensitized Solar Cells Based on Titania Nanotube Array Electrodes. *Nanotechnology* **2006**, *17*, 1446−1448.

(20) Shankar, K.; Mor, G. K.; Prakasam, H. E.; Yoriya, S.; Paulose, M.; Varghese, O. K.; Grimes, C. A. Highly-Ordered TiO_2 Nanotube Arrays up to 220 μm in Length: Use in Water Photoelectrolysis and Dye-Sensitized Solar Cells. *Nanotechnology* **2007**, *18*, 65707−65718.

(21) Park, J. H.; Lee, T. W.; Kang, M. G. Growth, Detachment and Transfer of Highly-Ordered TiO_2 Nanotube Arrays Use in Dye-Sensitized Solar Cells. *Chem. Commun.* **2008**, *25*, 2867−2869.

(22) Chen, Q.; Xu, D. Large-Scale, Noncurling, and Free-Standing Crystallized TiO_2 Nanotube Arrays for Dye-Sensitized Solar Cells. *J. Phys. Chem. C* **2009**, *113*, 6310−6314.

(23) Lei, B. X.; Liao, J. Y.; Zhang, R.; Wang, J.; Su, C. Y.; Kuang, D. B. Ordered Crystalline TiO_2 Nanotube Arrays on Transparent FTO Glass for Efficient Dye-Sensitized Solar Cells. *J. Phys. Chem. C* **2010**, *114*, 15228−15233.

(24) Albu, S. P.; Ghicov, A.; Macak, J. M.; Hahn, R.; Schmuki, P. Self-Organized, Free-Standing TiO_2 Nanotube Membrane for Flow-through Photocatalytic Applications. *Nano Lett.* **2007**, *7*, 1286−1289.

(25) Li, L. L.; Chen, Y. J.; Wu, H. P.; Wang, N. S.; Diau, E. G. Detachment and Transfer of Ordered TiO_2 Nanotube Arrays for Front-Illuminated Dye-Sensitized Solar Cells. *Energy Environ. Sci.* **2011**, *4*, 3420−3425.

(26) Yip, C.-T.; Guo, M.; Huang, H.; Zhou, L.; Wang, Y.; Huang, C. Open-Ended TiO_2 Nanotubes Formed by Two-Step Anodization and Their Application in Dye-Sensitized Solar Cells. *Nanoscale* **2012**, *4*, 448−450.

(27) Lin, C. J.; Yu, W. Y.; Chien, S. H. Transparent Electrodes of Ordered Opened-End TiO_2-Nanotube Arrays for Highly Efficient Dye-Sensitized Solar Cells. *J. Mater. Chem.* **2010**, *20*, 1073−1077.

(28) Chen, C. C.; Chung, H. W.; Chen, C. H.; Lu, H. P.; Lan, C. M.; Chen, S. F.; Luo, L.; Hung, C. H.; Diau, E. W. Fabrication and Characterization of Anodic Titanium Oxide Nanotube Arrays of Controlled Length for Highly Efficient Dye-Sensitized Solar Cells. *J. Phys. Chem. C* **2008**, *112*, 19151−19157.

(29) Roy, R.; Kim, D.; Paramasivam, I.; Schmuki, P. Improved Efficiency of TiO_2 Nanotubes in Dye-Sensitized Solar Cells by

Decoration with TiO_2 Nanoparticles. *Electrochem. Commun.* **2009**, *11*, 1001−1004.
(30) Lin, J.; Liu, X.; Guo, M.; Lu, W.; Zhang, G.; Zhou, L.; Chen, X.; Huang, H. A Facile Route to Fabricate an Anodic TiO_2 Nanotube−Nanoparticle Hybrid Structure for High Efficiency Dye-Sensitized Solar Cells. *Nanoscale* **2012**, *4*, 5148−5153.
(31) Choi, J.; Park, S.-H.; Kwon, Y. S.; Lim, J.; Song, I. Y.; Park, T. Facile Fabrication of Aligned Doubly Open-Ended TiO_2 Nanotubes, via a Selective Etching Process, for Use in Front-Illuminated Dye-Sensitized Solar Cells. *Chem. Commun.* **2012**, *48*, 8748−8750.
(32) Park, S.-H.; Lim, J.; Kwon, Y. S.; Song, I. Y.; Choi, J.; Song, S.; Park, T. Tunable Nanoporous Network Polymer Nanocomposites having Size-Selective Ion Transfer for Dye-sensitized Solar Cells. *Adv. Energy Mater.* **2013**, *3*, 184−192.
(33) Kwon, Y. S.; Song, I.; Lim, J.; Song, I. Y.; Siva, A.; Park, T. Exploring the Heterogeneous Interfaces in Organic or Ruthenium Dye-Sensitized Liquid- and Solid-State Solar Cells. *ACS Appl. Mater. Interfaces* **2012**, *4*, 3141−3147.
(34) Park, S.-H.; Lim, J.; Song, I. Y.; Lee, J.-R.; Park, T. Physically Stable Polymer-Membrane Electrolytes for Highly Efficient Solid-State Dye-Sensitized Solar Cells with Long-Term Stability. *Adv. Energy Mater.* **2014**, DOI: 10.1002/aenm.201470013.
(35) Huang, S. Y.; Schlichthörl, G.; Nozik, A. J.; Grätzel, M.; Frank, A. J. Charge Recombination in Dye-Sensitized Nanocrystalline TiO_2 Solar Cells. *J. Phys. Chem. B* **1997**, *101*, 2576−2582.
(36) Koster, L. J. A.; Mihailetchi, V. D.; Ramaker, R.; Blom, P. W. M. Light Intensity Dependence of Open-Circuit Voltage of Polymer:-Fullerene Solar Cells. *Appl. Phys. Lett.* **2005**, *86*, 123509−123511.
(37) Wang, Z.-S.; Kawauchi, H.; Kashima, T.; Arakawa, H. Significant Influence of TiO_2 Photoelectrode Morphology on The Energy Conversion Efficiency of N719 Dye-Sensitized Solar Cell. *Coord. Chem. Rev.* **2004**, *248*, 1381−1389.
(38) Mor, G. K.; Shankar, K.; Paulose, M.; Varghese, O. K.; Grimes, C. A. Use of Highly-Ordered TiO_2 Nanotube Arrays in Dye-Sensitized Solar Cells. *Nano Lett.* **2006**, *6*, 215−218.
(39) Kwon, Y. S.; Lim, J.; Song, I.; Song, I. Y.; Shin, W. S.; Moon, S.-J.; Park, T. Chemical Compatibility between A Hole Conductor and Organic Dye Enhances The Photovoltaic Performance of Solid-State Dye-Sensitized Solar Cells. *J. Mater. Chem.* **2012**, *22*, 8641−8648.
(40) Kwon, Y. S.; Song, I. Y.; Lim, J.; Park, S.-H.; Siva, A.; Park, Y.-C.; Jang, H. M.; Park, T. Reduced Charge Recombination by the Formation of an Interlayer Using a Novel Dendron Coadsorbent in Solid-State Dye-Sensitized Solar Cells. *RSC Adv.* **2012**, *2*, 3467−3472.